Spectral curves of surface reflectance in some Antarctic regions (*)

A. Lupi[1], C. Tomasi[1], A. Orsini[1], A. Cacciari[1]
V. Vitale[1], T. Georgiadis[1], R. Casacchia[2]
R. Salvatori[2] and S. Salvi[3]

[1] *Institute of Atmospheric and Oceanic Sciences (ISAO) - CNR*
  Via Gobetti 101, I-40129 Bologna, Italy
[2] *Institute for Atmospheric Pollution (IIA) - CNR*
  Via Salaria 29.3 km, I-00016 Monterotondo Scalo (Roma), Italy
[3] *National Institute of Geophysics (ING), Remote Sensing Laboratory*
  Via di Vigna Murata 605, I-00143 Roma, Italy

Summary. — Four surface reflectance models of solar radiation were determined by examining several sets of field measurements taken for clear-sky conditions at various sites in Antarctica. Each model consists of the mean spectral curve of surface reflectance in the 0.25–2.7 μm wavelength range and of the dependence curve of total albedo on the solar elevation angle h, within the range from $5°$ to $55°$. The TNB (Terra Nova Bay) model refers to a rocky terrain where granites are predominant; the NIS (Nansen Ice Sheet) model to a glacier surface made uneven by sastrugi and streaked by irregular fractures; the HAP (High Altitude Plateau) model to a flat ice surface covered by fresh snow and scored by light sastrugi; and the RIS (Ross Ice Shelf) model to an area covered by the sea ice pack presenting many discontinuities in the reflectance features, due to melt water lakes, puddles, refrozen ice and snow pots. The reflectance curve obtained for the TNB model presents gradually increasing values as wavelength increases through the visible spectral range and almost constant values at infrared wavelengths, giving a total albedo value equal to 0.264 at $h = 30°$, which increases by about 80% through the lower range of h and decreases by 12% through the upper range. The reflectance curves of the NIS, HAP and RIS models are all peaked at visible wavelengths and exhibit decreasing values throughout the infrared spectral range, giving values of total albedo equal to 0.464, 0.738 and 0.426 at $h = 30°$, respectively. These values were estimated to increase by 8–14% as h decreases from $30°$ to $5°$ and to decrease by 2–4% only as h increases from $30°$ to $55°$.

PACS 92.60 – Meteorology.
PACS 42.68 – Atmospheric optics.
PACS 94.10 – Physics of the neutral atmosphere.

1. – Introduction

In Antarctica, the area covered by ice and snow varies on the average from less than 5 million square kilometers in the January-March period to more than 15 million square kilometers in the July-September period, presenting mean yearly values of the surface albedo higher than 0.8 in all the land regions [1]. Since surface albedo is given by the ratio of the wavelength-averaged solar radiation reflected by the terrestrial surface to that incident on it, Antarctica turns out to be one of the planetary areas with the most important influence on the Earth radiation budget. Thus, surface albedo is a very significant parameter for determining the albedo of the whole surface-atmosphere system and the radiative forcing effects produced by aerosol particles of both natural and anthropic origins. Paltridge and Platt [2] showed that the same columnar content of aerosol particles can produce changes of opposite sign in the surface-atmosphere albedo, when the particulate matter is suspended over a low-albedo surface, like that of the sea surface, or a high-albedo surface like that of the continental ice cap covering Antarctica. More generally, in the surface-atmosphere system where multiple reflection processes of solar radiation take place due to both Rayleigh and aerosol scattering, the planetary reflectance strongly depends on the surface reflectance characteristics and scattering properties of aerosol particles [3]. Therefore, in order to obtain correct evaluations of the instantaneous direct radiative forcing caused by aerosol particles, it is of basic importance to know not only the radiative properties of aerosol particles but also the spectral features of surface reflectance together with its dependence patterns on the solar elevation angle.

Appropriate and precise models of surface reflectance are herein defined within the solar radiation spectral range and for clear-sky conditions, also including the dependence features of surface reflectance on both wavelength and solar elevation angle, from which realistic evaluations of the instantaneous direct radiative forcing caused by aerosol particles in Antarctica can be obtained [4].

2. – The choice of study areas

Considering the Antarctic region surrounding the Terra Nova Bay station and the surface characteristics most frequently observed in that part of the continent during the period of maximum insolation, from November to February, we chose four areas presenting well-defined characteristics of the surface, associated with marked differences in the spectral reflectance characteristics, covering a wide range of the surface albedo. They are:

1) The Terra Nova Bay (TNB) area (74°42′ S; 164°07′ E) including the coastal region of the Northern Foothills located between the Campbell and Drygalski glacier tongues. In this area, the field station of Campo Icaro (74°43′ S; 164°07′ E) is also located at an altitude of 50 m a.m.s.l. on a promontory presenting a surface completely de-iced during the warmer months. The area is characterized by a heterogeneous soil morphology. For instance, large regions exhibit rocky formations with a prevailing presence of syenogranites, like those observable at the sites of Inexpressible Island, Mount Gerlache and Terra Nova Bay station, while formations of amphiboles and biotite quartzdiorites outcrop at Teall Nunatak [5].

2) The confluence area of the Reeves glacier (74°39′ S; 161°35′ E) with the Nansen Ice Sheet (NIS) (74°52′ S; 163°00′ E). The latter area is a permanently frozen branch of the Ross Sea bordered by the Northern Foothills on the east, confined by the open sea on the south and south-west during the November-February period and surrounded on the west

and north sides by a mountainous land steeply rising towards the Antarctic Plateau. The Prestley glacier descends from the north along a gently sloping valley, while the Reeves glacier reaches the Nansen Ice Sheet descending from north-west along a large and steep valley. Therefore, the NIS area exhibits a very heterogeneous surface, characterized by irregular and diverse spectral characteristics due to the presence of an ice cover intersected by crevasses and scratched by sastrugi of different sizes, which are wind-formed minor reliefs with orientation defined by the direction of the katabatic winds which generated them [6]. Most of the NIS area is often covered by thin layers of fresh snow also during the summer months, which considerably strengthen the reflectance properties. The central-eastern region presents large areas of bare ice, due to the persistent katabatic winds blowing down the Prestley and Reeves valleys. Moreover, lakes of large sizes can be formed in this region during the summer period, due to ice melting [7].

3) An area of the Antarctic Plateau, characterized by a flat glacial surface irregularly covered by uniform layers of fresh snow and sometimes by dry windpacked snow, forming irregular and small sastrugi. Similar characteristics are typical of the wide regions of the high altitude plateau (HAP), where the meteorological conditions favour the formation of these irregular ice and snow reliefs whose size is generally smaller in areas not swept by strong katabatic winds and whose shapes are modelled by aeolian-forced processes, including both deposition and erosion effects [6].

4) An area of the Ross Ice Shelf (RIS), that is part of the Ross Sea which more deeply penetrates the Antarctic continent. The area is permanently covered by a surface ice layer, which usually presents different spectral reflectance features, since the ice coverage is partly melted or re-frozen during the summer and partly covered by snow pots of various age, characterized by different structural features.

3. – The TNB model

In order to define the average spectral curve of surface reflectance $R(\lambda)$ suitable for the TNB model, we considered the following sets of spectral measurements:

1) the surface reflectance curve used by Vermote *et al.* [8] in the 6S computer code within the 0.3–2.3 μm wavelength range to represent the dry-sand surface;

2) the average spectral curve of soil reflectance determined by Tomasi *et al.* [9] in the 0.3–1.2 μm wavelength range (for solar elevation angle $h = 30°$) in order to define a sky radiance model at the Campo Icaro station;

3) the spectral series of bihemispherical reflectance determined by Zibordi and Meloni [5] in the 0.555–0.89 μm wavelength range (more precisely, at the four central wavelengths of the Landsat-TM radiometric channels, equal to 0.555, 0.649, 0.749 and 0.892 μm) from exitance and irradiance measurements taken at $h = 29°$ with the Exotech 100 A radiometer in an area with syenogranites near the Terra Nova Bay station;

4) the spectral series of mean reflectance obtained by Casacchia *et al.* [10] in the 0.555–0.892 μm wavelength interval from Landsat-TM and SPOT-XS processed images and radiometric field data taken with the Exotech 100 A radiometer in areas with granite outcrops; and

5) the spectral curve of surface reflectance $R(\lambda)$ obtained by averaging three spectral curves determined by us from solar irradiance measurements taken with a portable Field-Spec spectroradiometer within the 0.35–2.50 μm wavelength range at Campo Oasi, near the Terra Nova Bay station, for clear-sky conditions ($h = 36°48'$) in a rocky area characterised by the predominant presence of leucogranites with centimeter-sized irregularities due to protruding feldspar crystals.
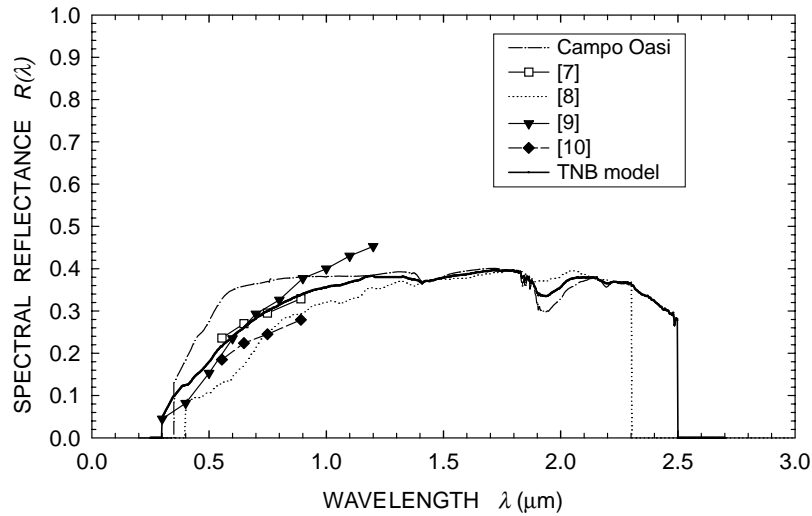
Fig. 1. – Spectral curves of surface reflectance $R(\lambda)$ obtained from our measurements performed at Campo Oasi and other field measurements [7-10], from which the average curve adopted in the TNB model within the 0.25–2.7 μm wavelength range was determined.

All these spectral data-sets are shown in fig. 1. The values of $R(\lambda)$ were used to calculate the mean curve of surface reflectance in wavelength steps of 1 nm. This curve, adopted to represent the surface reflectance characteristics at $h = 30°$ in the TNB model, is shown in fig. 1: it presents rapidly increasing values throughout the visible wavelength range and almost neutral spectral dependence features in the infrared. This reflectance model needs to be completed with the dependence curve of surface reflectance on the solar elevation angle. Theoretical studies made by Choudhury and Chang [11] on the spectral characteristics of snow surfaces with different grain sizes indicate that $R(\lambda)$ should vary as a function of h following a trend varying with wavelength. In fact, the results found by Choudhury and Chang [11] show that the snow reflectance varies very little throughout the range $20° \leq h \leq 40°$ at visible wavelengths and more widely at infrared wavelengths $\lambda > 1\,\mu$m. However, it is important to take into account that i) the prevailing fraction of solar radiation reaching the ground at Antarctic stations (at $h = 30°$) is found within the spectral range from 0.38 to 1 μm (our calculations made for the "January, 75° S" atmospheric model [12] indicate a percentage of 69.2%, while 3.7% pertains to the range $\lambda < 0.38\,\mu$m and 27.1% to the range $\lambda > 1\,\mu$m, and ii) the total albedo A is given by the mean value of the integral of $R(\lambda)$ calculated throughout the whole solar spectrum. On the basis of these remarks, we assumed in our models that total albedo varies as a function of h following an average trend very close to that followed on the average by the monochromatic components of reflectance $R(\lambda)$ in the visible and near-infrared spectral range. This approximated assumption appears to be fair, yielding realistic results for all the surface kinds.

Thus, in order to define the angular dependence features of $R(\lambda)$ in the TNB model, we considered two angular dependence curves of A on the solar elevation angle h: i) one proposed by Iqbal [13] for a desert dust surface, and ii) one defined from the measurements taken by Idso *et al.* [14] for a dry soil surface. The choice of the first curve was made considering that the reflectance curve of the dry sand surface shown in fig. 1 presents very

TABLE I. – *Values of the angular correction factor $f(h)$ for eleven values of solar elevation angle h from $5°$ to $55°$ and for the four reflectance models defined in the present study.*

Solar elevation angle h (degrees)	Angular correction factor $f(h)$			
	TNB model	NIS model	HAP model	RIS model
5	1.805	1.082	1.110	1.141
10	1.509	1.057	1.070	1.093
15	1.289	1.037	1.042	1.057
20	1.159	1.022	1.022	1.032
25	1.074	1.010	1.009	1.014
30	1.000	1.000	1.000	1.000
35	0.960	0.991	0.993	0.990
40	0.935	0.982	0.988	0.981
45	0.912	0.975	0.984	0.973
50	0.898	0.970	0.980	0.968
55	0.885	0.965	0.977	0.963

similar spectral features to those of the TNB curve. The angular dependence curve of A given by Iqbal [13] exhibits values decreasing from about 0.650 to 0.326 as h increases from $5°$ to $30°$ and slowly decreasing values throughout the upper range, reaching 0.282 at $h = 55°$. The values of A derived from the curve of Idso *et al.* [14] were found to decrease from 0.511 to 0.320 as h increases from $5°$ to $30°$ and to decrease further throughout the upper range until reaching 0.290 at $h = 55°$. The values of A given by the two curves were used to calculate the corresponding average values of $A(h)$, from which the average values of $f(h)$, assumed to be equal to the ratio $A(h)/A(30°)$, were determined at eleven values of h, as given in table I. On the basis of the above assumption, the TNB reflectance curves can be determined at the various solar elevation angles by multiplying the monochromatic values of the TNB surface reflectance curve shown in fig. 1 at $h = 30°$ by the corresponding values of correction factor $f(h)$, as calculated through linear interpolation between the values given in table I.

4. – The NIS model

The spectral curve of surface reflectance $R(\lambda)$ for the NIS model was determined from the following data-sets:

1) the spectral curve of $R(\lambda)$ defined by Tomasi *et al.* [9] for a clean snow surface ($h = 30°$) in the 0.3–0.5 μm wavelength interval;

2) the spectral series of bihemispherical reflectance obtained by Zibordi and Meloni [5] at four wavelengths in the 0.555–0.892 μm range, from measurements taken at the Prestley glacier in a surface of outlet glacier blue ice ($h = 33°$);

3) two spectral curves of $R(\lambda)$ determined by Zibordi *et al.* [7] in the 0.45–2.5 μm wavelength range from measurements taken in a glacier ice surface covered by a dusting of snow ($h = 32°32'$) and a glacier ice surface ($h = 33°59'$), respectively;

4) five spectral curves of $R(\lambda)$ measured by us in the 0.35–2.5 μm spectral range for clear-sky conditions at i) the Browning Pass (240 m a.m.s.l.), for an irregular surface of white ice with isolated snow inclusions ($h = 34°$), ii) the Campbell Glacier (2 m a.m.s.l.), for a regular azure-white ice pack surface without fractures ($h = 30°$), iii) a site of Terra
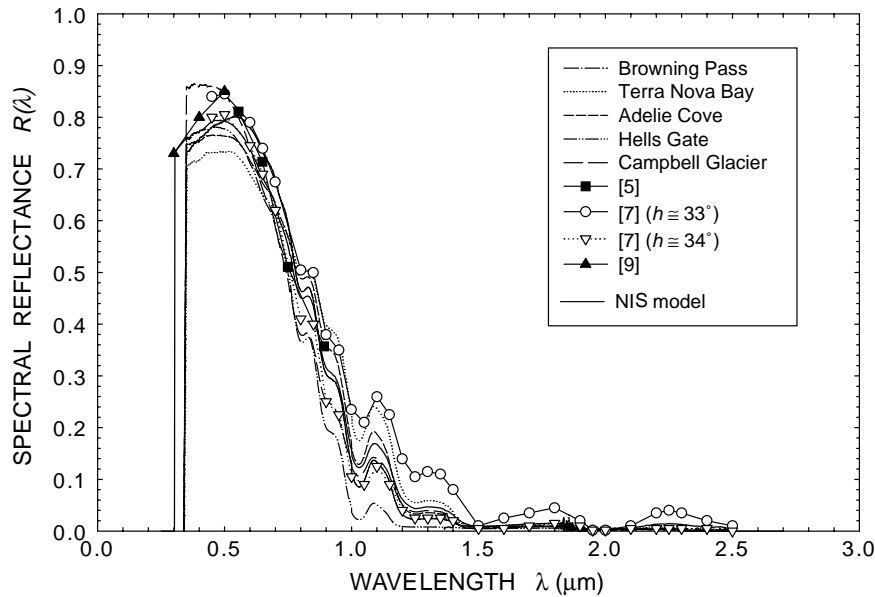
Fig. 2. – Spectral curves of surface reflectance $R(\lambda)$ obtained from our measurements performed at five different sites and other field measurements [5,7,9], from which the average curve adopted in the NIS model within the 0.25–2.7 μm wavelength range was determined.

Nova Bay near the coast, for a smooth white ice pack ($h = 34°$), iv) the Adelie Cove (2 m a.m.s.l.), for a white pack surface ($h = 34°$), and v) the Hells Gate (sea-level), for a glacier surface consisting of pale azure ice presenting a two-layer coverage with an upper colourless layer of about 5 cm depth and a lower layer containing small snow inclusions ($h = 31°$).

The above nine spectral curves of $R(\lambda)$ are shown in fig. 2. From them, we determined the average spectral curve of $R(\lambda)$ for the NIS model, which was assumed to be valid for $h = 30°$. The curve, shown in fig. 2, exhibits a peaked shape in the visible and decreases rapidly throughout the near-infrared spectral range to reach values close to zero beyond the 1.5 μm wavelength. Following the same procedure adopted above for determining the mean angular dependence curve of surface albedo A in the TNB model, we considered the following data-sets shown in fig. 3: i) the angular dependence curve of total albedo A given by Rusin [15] for a snow surface; ii) the angular dependence curve of A obtained by Choudhury and Chang [11] from snow surface models with different grain sizes; iii) the angular dependence curve of A proposed by Iqbal [13] for a snow surface; and iv) the angular dependence curve of A determined by us from total albedo measurements taken on four days of November and December 1994 at the Reeves Nevè for different values of both solar elevation and azimuth angles [16].

This last curve was obtained from the field measurements mentioned above. Figure 4 shows those taken on two days only, indicating very clearly that the surface albedo A can assume different values during the day, for the same value of solar elevation angle h but for different values of the solar azimuth angle φ. Such behaviour can be reasonably explained as being due to the particular orientation of sastrugi with respect to the incoming solar radiation. In fact, these reliefs are mainly formed by wind-modelling of the snow cover
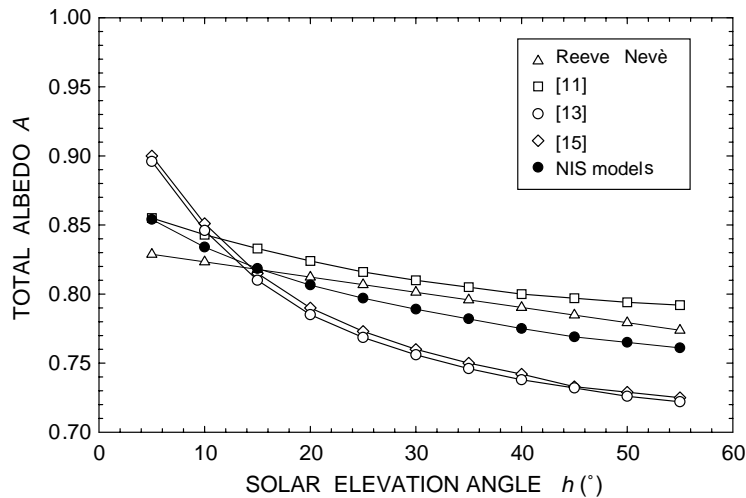
Fig. 3. – Angular dependence curves of total albedo A obtained from the Reeves Nevè glacier measurements and snow-covered surface albedo models [11,13,15], from which the average curve adopted in the NIS model was determined.

and, consequently, present a predominant orientation in the direction defined by the local katabatic winds. Thus, appreciable changes in the percentage of the surface not directly illuminated by the sun light can occur as the solar azimuth angle varies during the day. All the measurements of total albedo A carried out on the four days are plotted in fig. 5(a) as a function of h, providing evidence of the large scatter of data caused by the changes in the shade fraction of the surface depending on the variations of the sun coordinates. From these data, we calculated the four-day mean values of A over sub-intervals $\Delta\varphi = 2.5°$ (separately considered for values of φ smaller and greater than $180°$) and sub-intervals $\Delta h = 1°$. The mean values of A are shown in fig. 5(b) together with their standard deviations, separately for $\varphi < 180°$ and $\varphi > 180°$, clearly indicating that the values of A found for values of $\varphi > 180°$ decrease from about 0.87 to 0.80 throughout the range of h from $6°$ to about $35°$, while those found for $\varphi < 180°$ turn out to decrease sharply below 0.75 and, subsequently, to gradually increase, reaching a value higher than 0.78 at $h = 37°$. The average dependence of A on solar elevation angle h was determined for the whole set of measurements shown in fig. 5(b), finding that the average values of A follow a slowly decreasing and nearly linear trend through the range of h from about $6°$ to $37°$. The average values are shown in fig. 5(b), together with their standard deviations and the regression line which represents very well such a linear trend, as it has intercept value equal to 0.834 and slope coefficient equal to -0.0011 $(°)^{-1}$, found for a regression coefficient equal to -0.931. The corresponding best-fit line is also shown in fig. 3 for comparison with the three other angular dependence curves of A found in the literature.

From these four curves of $A(h)$, we calculated the average NIS curve of $A(h)$ shown in fig. 3 within the range $5° < h < 60°$, from which the NIS values of the correction factor $f(h)$ were determined, as given in table I.
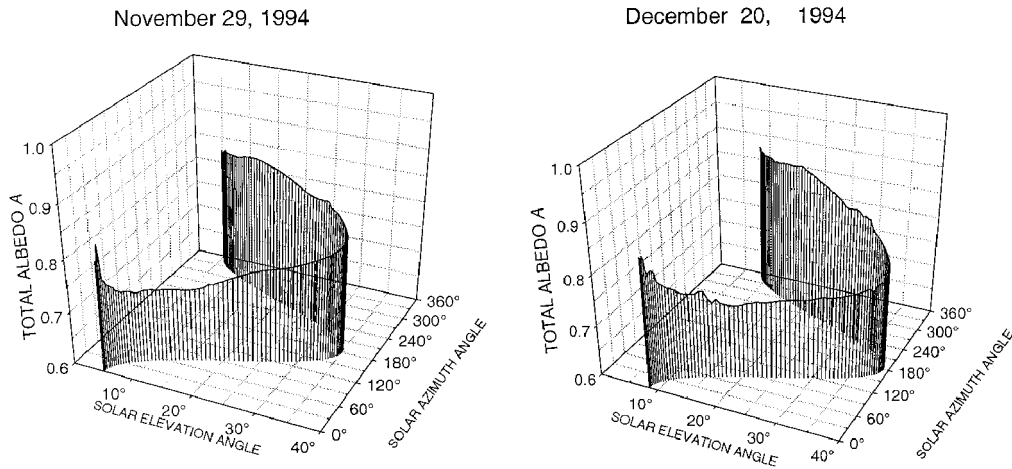
November 29, 1994   December 20, 1994

Fig. 4. – Three-dimensional curves of total albedo A as a function of solar elevation angle h and solar azimuth angle φ, as measured at the Reeves Nevè glacier on two of the four measurement days [16].

5. – The HAP model

The spectral curve of $R(\lambda)$ for the HAP model was calculated from following data-sets:

1) the theoretical curve of $R(\lambda)$ calculated by Choudhury and Chang [11] at $h = 30°$, using snow surface models with grain sizes of $0.2\,\mathrm{mm}$;

2) the spectral series of bihemispherical reflectance determined by Zibordi and Mel-
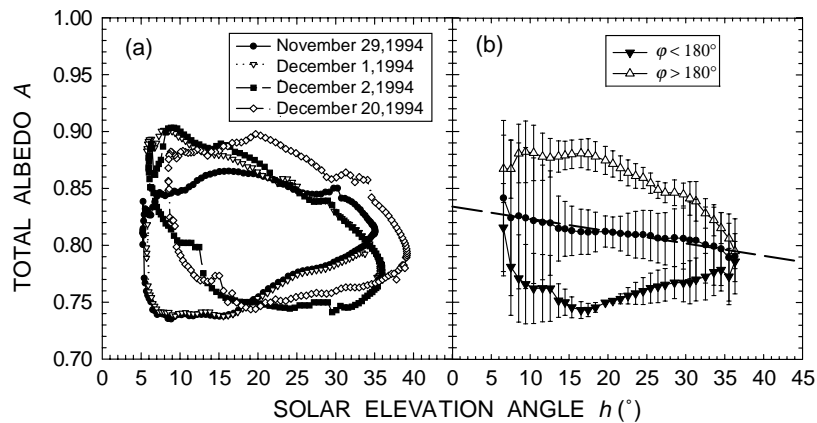
Fig. 5. – Part (a): total albedo A as a function of solar elevation angle h, as found from the measurements taken at the Reeves Nevè glacier on four days of 1994. Part (b): mean values of A plotted as a function of h, as obtained separately for the two sets $\varphi < 180°$ and $\varphi > 180°$ and intervals $\Delta h = 1°$, together with their standard deviations. The overall mean values of A (solid circles) are also shown together with their standard deviations and the regression line (dashed line) fitting them.

oni [5] at four visible and near-infrared wavelengths from radiometric measurements carried out at the Tourmaline Plateau (about 1700 m a.m.s.l.) on a surface covered by fresh snow ($h = 33°$);

3) the spectral reflectance curve found by Zibordi *et al.* [7] from measurements taken at the Hercules Nevè (2990 m a.m.s.l.) on a snow surface with grain sizes of 0.2–0.3 mm ($h = 31°12'$);

4) the spectral curve of $R(\lambda)$ determined by Zibordi *et al.* [7] in the 0.45–2.5 μm wave-length range for a glacier ice surface covered by a snowpack layer of 1–2 cm depth ($h = 37°10'$);

5) three spectral curves of $R(\lambda)$ measured by us with the FieldSpec spectroradiometer in the 0.35–2.5 μm spectral range for clear-sky conditions, two of which at the Tourmaline Plateau (1637 m a.m.s.l.) for regular surfaces in open areas, both presenting solid faceted and small rounded ice particles of around 0.2 mm sizes (with $h = 31°$ and $h = 32°$, respectively), and the third one at the Browning Pass (250 m a.m.s.l.) for a rough surface covered by drifted snow containing small rounded particles of 0.2 mm sizes ($h = 32°$).

The seven spectral curves of $R(\lambda)$ are shown in fig. 6, presenting a homogeneous picture of the spectral characteristics of surface reflectance observed in high altitude plateau regions, which agree very well with the spectral reflectance curve theoretically defined by Choudhury and Chang [11] for a clean snow surface. The mean spectral curve of surface reflectance for the HAP model was determined by averaging the spectral reflectance values given by the seven curves shown in fig. 6. This average curve presents very high values within the entire visible spectral range and decreasing values throughout the near-infrared wavelength range. Considering that the experimental data sets were taken for solar elevation angles mostly ranging between 30° and 33°, we decided to assume that the average reflectance curve of the HAP model is valid for $h = 30°$.

The angular dependence features of total albedo A in the HAP model were determined from the following data sets shown in fig. 7 within the range of h from 5° to 55°: i) the four curves of $A(h)$ derived from the total albedo measurements taken by Carroll and Fitch [17] within the 0.28–2.8 μm wavelength range at the four high-altitude Antarctic stations of Charcot (2400 m a.m.s.l.), Pionerskaya (2740 m a.m.s.l.), Vostok II (3488 m a.m.s.l.) and Plateau (3625 m a.m.s.l.), for both clear sky conditions and cloudiness of less than 0.25; and ii) the theoretical curve evaluated by Choudhury and Chang [11] for a clean snow surface containing grains of 0.2 mm sizes. The comparison shows that the experimental data are not far from those theoretically defined by Choudhury and Chang [11]. Therefore, we calculated the average curve of $A(h)$ from these five curves, as shown in fig. 7 as the HAP curve, and used it for calculating the values of $f(h)$ given in table I for the HAP model. It is important to notice that the values of $R(\lambda)$ at visible wavelengths are all higher than 0.9 and, hence, the products of $R(\lambda)$ by $f(h)$ at $h = 5°$ turn out to be greater than one: in these cases, we are obliged to assume $R(\lambda)$ as equal to one for practical purposes.

6. – The RIS model

In order to determine the spectral curve of $R(\lambda)$ for the RIS model, we examined the following sets of field measurements:

1) the spectral curve determined by Tomasi *et al.* [9] within the 0.3–0.6 μm wavelength range for a snow surface ($h = 30°$);

2) the spectral curve defined by Zibordi and Marracci [18] from measurements taken in a sea ice surface ($h = 32°$);
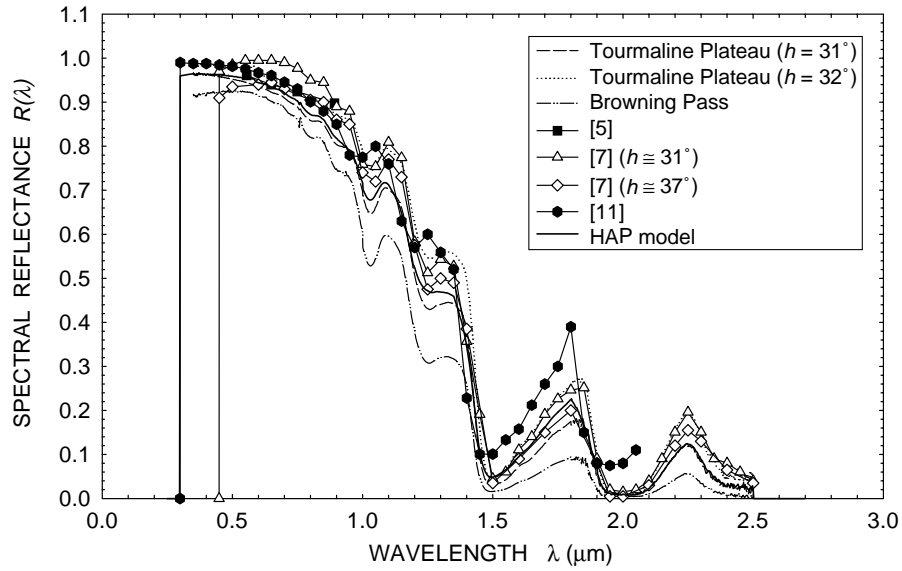
Fig. 6. – Spectral curves of surface reflectance $R(\lambda)$ obtained from our measurements performed at two high-altitude sites, other field measurements [5, 7] and surface reflectance models [11], from which the average curve adopted in the HAP model within the 0.25–2.7 μm wavelength range was determined.
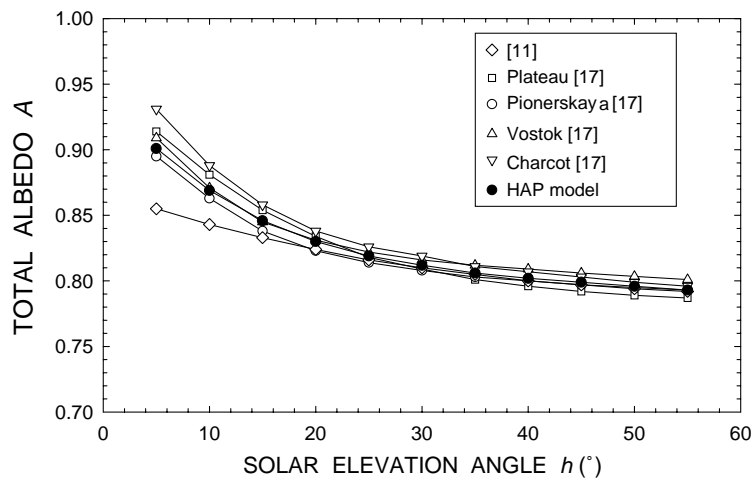

Fig. 7. – Angular dependence curves of total albedo A obtained from surface albedo models [11] and field measurements [17], from which the average curve adopted in the HAP model was determined.
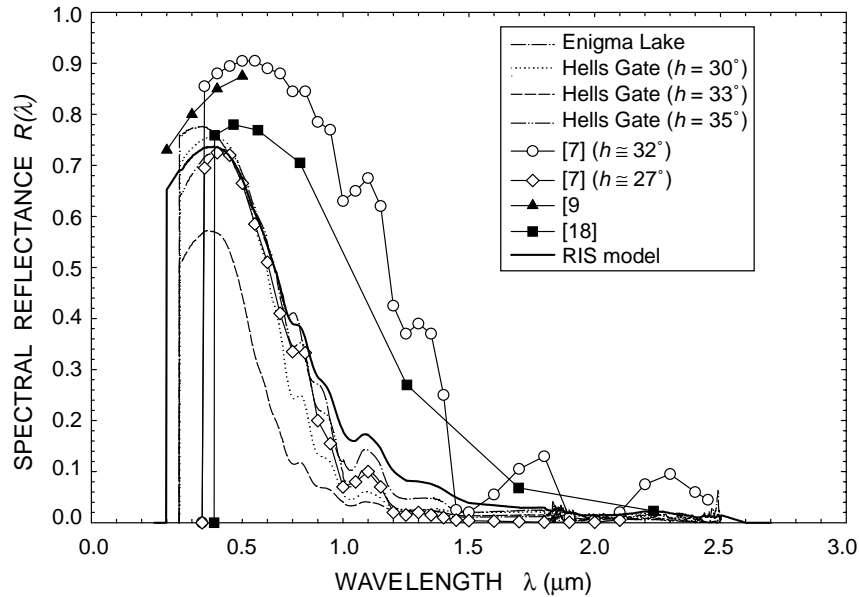
Fig. 8. – Spectral curves of surface reflectance $R(\lambda)$ obtained from our measurements performed at two coastal sites and from other field measurements [7, 9, 18], from which the average curve adopted in the RIS model within the 0.25–2.7 μm wavelength range was determined.

3) two spectral curves measured by Zibordi *et al.* [7], the first for a lake ice area covered by a snowpack of 2–3 cm depth ($h = 32°$) and the second for a re-frozen lake ice surface ($h = 27°20'$);

4) four spectral curves of $R(\lambda)$ measured by us with the FieldSpec spectroradiometer in the 0.35–2.5 μm spectral range, the first at the Enigma Lake (180 m a.m.s.l.), for a rough surface of colourless lake ice including many hexagonal snow features of 5–10 mm size ($h = 32°$), and the three other at Hells Gate (20 m a.m.s.l.) for an open wide area covered by azure ice with snow inclusions of 10–15 mm sizes ($h = 30°$), an open wide area presenting azure ice with surface impurities ($h = 33°$) and a melt water lake ice surface, containing azure ice with small spheroidal snow-inclusions of about 2 mm sizes and other larger snow-inclusions ($h = 35°$), respectively.

These eight spectral curves of $R(\lambda)$ are shown in fig. 8. The comparison gives evidence of the large discrepancies which can be caused by the very different morphological and radiative characteristics shown by the various surfaces in the RIS area, because of the formation of melt water lakes or the presence of different surface texture features in the broad areas covered by ice and snow and containing various dust intrusions producing peculiar optical effects. Therefore, we decided to calculate the average spectral curve of surface reflectance for the RIS model from this wide set of spectral curves, obtaining the average RIS curve of $R(\lambda)$ shown in fig. 8. This average curve, characterized by a peaked shape in the visible and by a rapidly decreasing wing throughout the near-infrared spectral range, was assumed to be valid for $h = 30°$, since all the eight experimental curves shown in fig. 8 were measured for values of h varying between 27° and 35°.

The angular dependence curve of $A(h)$ for the RIS model was determined from the data-sets shown in fig. 9: i) the angular dependence curve of A obtained by smoothing the
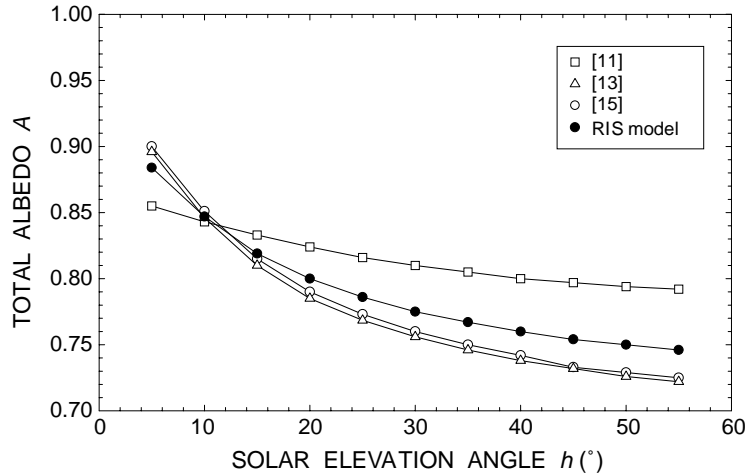
Fig. 9. – Angular dependence curves of total albedo A obtained from surface albedo models [11, 13,15], from which the average curve adopted in the RIS model was determined.

values given by Rusin [15]; ii) the thoretical curve defined by Choudhury and Chang [11] using various snow surface models; and iii) the angular dependence curve of total albedo proposed by Iqbal [13] for a snow surface. From these measurements, we calculated the average angular dependence curve of total albedo A shown in fig. 9 for the RIS model and the corresponding values of $f(h)$ given in table I.

7. – Conclusions

The evaluations of the wavelength dependence features of surface reflectance obtained for the four Antarctic areas considered in the present study are shown all together in fig. 10, so as to highlight their main characteristics and discrepancies throughout the wavelength range from 0.25 to 2.7 μm. As can be seen, there is a substantial difference between the TNB spectral curve of $R(\lambda)$, which presents relatively high and stable values at infrared wavelengths, and the three other curves, which are characterised by considerably higher values in the visible spectral range, although with different spectral features. In fact, the mean values of total albedo obtained by integrating the four curves shown in fig. 10 over the 0.25–2.7 μm wavelength range were found to be equal to 0.264 in the TNB model, 0.464 in the NIS model, 0.738 in the HAP model and 0.426 in the RIS model. Figure 10 also shows the spectral curve of $R(\lambda)$ for the clear (sea) water surface, as obtained by Vitale *et al.* [19] through corrections of the curve proposed by Vermote *et al.* [8], which take into account the evaluations of $R(\lambda)$ obtained with the Fresnel formula [20] using the monochromatic values of liquid water refractive index proposed by Irvine and Pollack [21]. Although obtained from spectral data sets found for largely different structure conditions of the surface in various Antarctic regions, the four spectral curves of $R(\lambda)$ can be reliably employed to evaluate the climatic effects caused by the various atmospheric constituents in the Antarctic surface-atmosphere system and, specifically, to obtain realistic estimates of the instantaneous direct radiative forcing produced by aerosols in the Antarctic regions and surrounding areas.

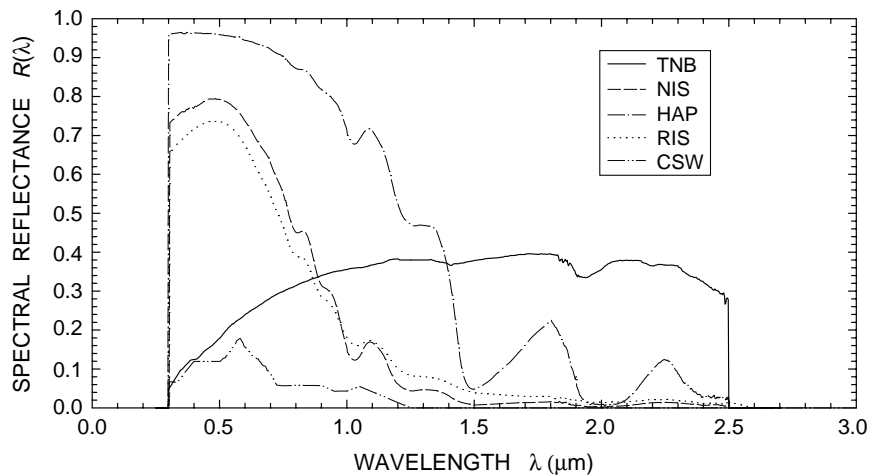The other important aspect when calculating the radiative forcing effects is the def-

Fig. 10. – Spectral curves of surface reflectance $R(\lambda)$ determined for the TNB, NIS, HAP and RIS models and the one defined by Vitale *et al.* [19] for the clear sea water (CSW) surface.

inition of the dependence curve of $R(\lambda)$ on the solar elevation angle. In this regard, we determined the dependence curves of total albedo A on h for the four Antarctic cases studied in the present paper, by multiplying the values of A obtained at $h = 30°$ as integrals of $R(\lambda)$ throughout the solar spectral range by the corresponding values of $f(h)$. The four curves of $A(h)$ determined applying this procedure to the TNB, NIS, HAP and RIS models are shown in fig. 11, together with the clear sea water (CSW) curve determined by Vitale *et al.* [19] through the analysis of the field measurements of total albedo A carried out by Kondratyev [22] for different sea-surface conditions and various
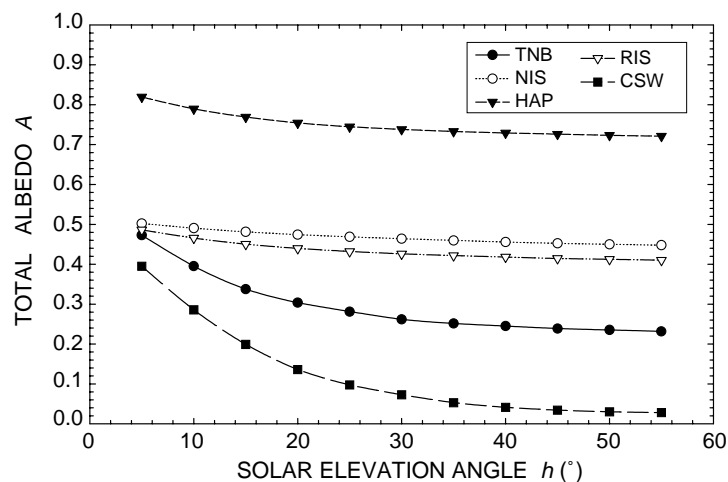

Fig. 11. – Angular dependence curves of total albedo A given in the TNB, NIS, HAP and RIS models together with the one proposed by Vitale *et al.* [19] for the clear sea water (CSW) surface model.
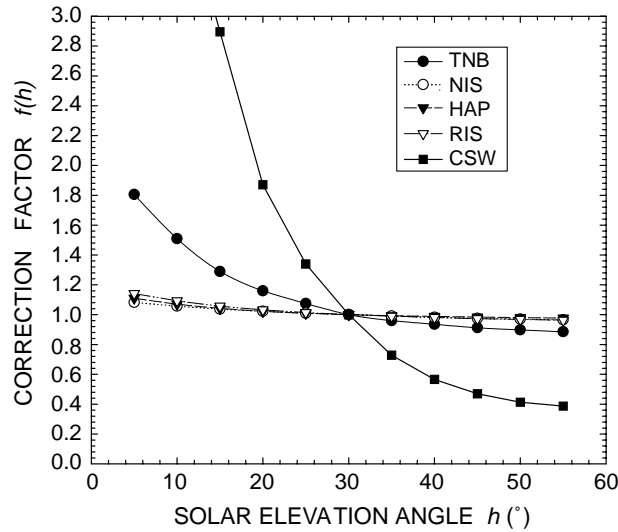
Fig. 12. – Angular dependence curves of correction factor $f(h)$ normalized to $h = 30°$, as determined for the TNB, NIS, HAP and RIS models and the clear sea water (CSW) surface model [19].

high-latitude oceanic regions. These results provide useful information on the angular dependence features of total albedo A of different surfaces and, hence, enable us to define with a good approximation the various surface reflectance models for application to climate studies.

In order to better define the average variations of A and $R(\lambda)$ due to changes in the solar elevation angle (based on the assumption that A and $R(\lambda)$ vary as a function of h following similar features), use was made of the mean values of angular correction factor $f(h)$ given in table I. These values are plotted in fig. 12 as a function of h for the four Antarctic models defined in the present study, as well as for the clear sea water surface (CSW) model mentioned above [19]. The accurate use of these parameters should allow us to obtain realistic evaluations of the changes in the surface reflectance characteristics occurring during the day and, consequently, of the instantaneous direct radiative forcing effects produced by aerosol particles.

$$* \ * \ *$$

REFERENCES

[1] HUMMEL J. R. and RECK R. A., *J. Appl. Meteor.*, **18** (1979) 239.
[2] PALTRIDGE G. W. and PLATT C. M. R., *Radiative Processes in Meteorology and Climatology* (Elsevier Sci. Publ. Co., Amsterdam) 1976, pp. 215-241.

[3] CHARLSON R. J., LANGNER J., RODHE H., LEOVY C. B. and WARREN S. G., *Tellus*, **43 AB** (1991) 152.

[4] CACCIARI A., TOMASI C., LUPI A., VITALE V. and MARANI S., *SIF Conf. Proc.*, Vol. **69** (Editrice Compositori, Bologna) 2000, p. 455.

[5] ZIBORDI G. and MELONI G. P., *Remote Sens. Environ.*, **37** (1991) 55.

[6] BROMWICH D. H., PARISH T. R. and ZORMAN C. A., *J. Geophys. Res.*, **95** (1990) 5495.

[7] ZIBORDI G., MELONI G. P. and FREZZOTTI M., *Cold Regions Sci. and Technol.*, **24** (1996) 147.

[8] VERMOTE E., TANRE' D., DEUZE' J. L., HERMAN M. and MORCRETTE J. J., *Second Simulation of the Satellite Signal in the Solar Spectrum (6S)*, 6S User Guide Version 2 (Lille, Universitè de Lille, France) 1997, p. 218.

[9] TOMASI C., VITALE V. and ZIBORDI G., *SIF Conf. Proc.*, Vol. **27** (Editrice Compositori, Bologna) 1990, p. 105.

[10] CASACCHIA R., MAZZARINI F., SALVATORI R. and SALVINI F., *Int. J. Remote Sensing*, **20** (1999) 403.

[11] CHOUDHURY B. J. and CHANG A. T. C., *J. Geophys. Res.*, **86** (1981) 465.

[12] TOMASI C. and VITALE V., *SIF Conf. Proc.*, Vol. **51** (Editrice Compositori, Bologna) 1996 p. 163.

[13] IQBAL M., *An Introduction to Solar Radiation* (Academic Press, Toronto) 1983, pp. 281-293.

[14] IDSO S. B., JACKSON R. D., REGINATO R. J., KIMBALL B. A. and NAKAYAMA F. S., *J. Appl. Meteor.*, **14** (1975) 109.

[15] RUSIN N. P., *Trans. Main Geophys. Obs.* No. 96 (1959).

[16] ORSINI A., CALZOLARI F., GEORGIADIS T., LEVIZZANI V., NARDINO M., PIRAZZINI R., RIZZI R., SOZZI R. and TOMASI C., *Atmos. Res.*, **54** (2000) 245.

[17] CARROLL J. J. and FITCH B. W., *J. Geophys. Res.*, **86** (1981) 5271.

[18] ZIBORDI G. and MARACCI G., *Remote Sens. Environ.*, **43** (1993) 11.

[19] VITALE V., TOMASI C., VON HOYNINGEN-HUENE W., BONAFE' U., MARANI S., LUPI A., CACCIARI A. and RUGGERI P., *Tellus B*, **52** (2000) 716.

[20] KONDRATYEV K. YA., *Radiation in the Atmosphere* (Academic Press, New York) 1969, pp. 411-452.

[21] IRVINE W. M. and POLLACK J. B., *Icarus*, **8** (1968) 324.

[22] KONDRATYEV K. YA., *Radiation Processes in the Atmosphere*, Second IMO Lecture, WMO - No. 309, 1972, p. 48.